Construction and Building Materials 230 (2020) 116898

Contents lists available at ScienceDirect

Construction and Building Materials

journal homepage: www.elsevier.com/locate/conbuildmat

Impact fatigue behaviour of GFRP mesh reinforced engineered cementitious composites for runway pavement

Yang Pan [a,1], Chao Wu [a,1], Xianfeng Cheng [b], Victor C. Li [c], Li He [d,*]

[a] School of Transportation Science and Engineering, Beihang University, 37 Xueyuan Road, Beijing 100191, China
[b] Hua Da Highway Engineering Consultant and Supervision Co., LTD., Tuanjie East Road No.21, Gaobeidian, Hebei 074000, China
[c] Department of Civil and Environmental Engineering, University of Michigan, Ann Arbor, 2350 Hayward St, Ann Arbor, MI 48109, USA
[d] School of Chemistry, Beihang University, 37 Xueyuan Road, Beijing 100191, China

HIGHLIGHTS

- Impact fatigue behavior of GFRP mesh reinforced ECC for runway pavement was studied.
- GFRP mesh reinforced ECC slab could sustain 30000 impacts at 3.6 MPa without failure.
- Ultrasonic testing method can be used to assess the damage status of the specimens.
- Ultrasonic testing method can predict the rest impact fatigue life of the specimens.

ARTICLE INFO

Article history:
Received 21 June 2019
Received in revised form 18 August 2019
Accepted 5 September 2019
Available online 18 September 2019

Keywords:
Cyclic impact
Runway pavement
Engineered cementitious composites (ECC)
Fiber reinforced polymer (FRP)
Composite

ABSTRACT

Concrete runway pavement faces a long term issue of cracking resulting in reduced durability and increased maintenance cost. This paper proposes a new type of runway pavement using engineered cementitious composites (ECC) with glass fiber reinforced polymer (GFRP) mesh reinforcements. This paper investigates the impact fatigue behaviour of the GFRP mesh reinforced ECC pavement through a series of cyclic impact tests. Five impact pressures were adopted considering the impacts induced by various types of airplanes. The number of impacts when the first crack appeared (N_0) and at the failure (N_C) were reported. The experimental results show that N_0 of GFRP mesh reinforced ECC is increased by a maximum of 800 times comparing to that of concrete pavement. The GFRP mesh reinforced ECC could sustain 30,000 impacts without failure. Finally, a non-destructive health monitoring algorithm was proposed based on the ultrasonic testing method and validated using the experimental results. This method is able to assess the damage status, and predict the remaining impact fatigue life of the GFRP mesh reinforced ECC pavement.

1. Introduction

Concrete pavement has been widely used in many international airports, but it faces a serious issue of cracking [1–5]. The cracking debris may destroy the engine of the airplane, and the annual engine maintenance cost could be several million dollars [6,7]. In addition, the repair of the cracked pavement would also incur delays and cancellations of flights [7–10].

Engineered cementitious composites (ECC) is a potential candidate material to solve the cracking issue of the concrete pavement. ECC is a cement based ductile material with a strain hardening behaviour in tension. Its strain capacity can reach up to 7% with multiple micro cracking with a width less than 60 μm [11]. Under bending load, an ECC slab can bend into a large curvature without brittle fracture. Therefore ECC is also called bendable concrete. ECC exhibits self-healing capacity making it a desirable material for sustainable pavement applications [11]. However, the tensile strength of ECC is similar to ordinary concrete [11–13] and internal reinforcements [14] are necessary. In recent years, glass fiber reinforced polymer (GFRP) mesh has been used as concrete reinforcements because of its advantages like high strength, low density and especially corrosion resistance in harsh environments [15–19]. Therefore, ECC reinforced with GFRP mesh is proposed as a runway pavement material in this paper. Considering the advantages of both composite materials, this GFRP mesh reinforced ECC runway pavement can be ductile with micro cracking and self-healing

* Corresponding author.
E-mail address: li_he@buaa.edu.cn (L. He).
[1] These authors have equal contribution.

https://doi.org/10.1016/j.conbuildmat.2019.116898
0950-0618/

behaviours. It is expected that the proposed runway pavement is more sustainable with improved serviceability and reduced life cycle maintenance costs.

Airport runways require sufficient impact fatigue performance to carry the massive cyclic pressure of the commercial aircrafts during their frequent takeoffs and landings [20]. However, to the best of the authors' knowledge, there is no available research in the literature about the impact fatigue behaviour of the runway pavement [21–28]. Although, a number of drop-weight impact tests have been conducted on concrete slabs these years, their experimental conditions, i.e. magnitude of the impact pressure, numbers of the cyclic pressure, were all different from those required by the runway pavement.

Ranade et al. [21] investigated the impact behaviour of high strength, high ductility concrete slabs which were placed on a steel frame holder. The size of the slab was 300 mm × 300 mm × 25 mm (thickness), and the impact pressure was from 12 MPa to 25 MPa applied with a metal head as the drop-weight. It was found that all slabs were broken within less than 20 impacts. Wu et al. [22] tested a composite pavement of three layers including an asphalt concrete layer (AC), a high strength concrete layer (HSC) and an ECC layer. The impact pressure was applied using an 1181 kg cylindrical projectile with a hemispheric metal head (100 mm in diameter). The shape and the material of the impact head in his study was quite different from the tyre of the aircraft. The size of the pavement specimen was 900 mm × 900 mm × 275 mm (thickness). The thickness of the AC, HSC and ECC was 75 mm, 100 mm and 100 mm, respectively. The specimen was put on a compacted sand base. The specimen was obviously damaged after the 2nd impact. Ramakrishna et al. [24] investigated the cyclic impact behaviour of fiber reinforced mortar slabs with a size of 300 mm × 300 mm × 20 mm (thickness). The slabs were simply supported on four edges, and a metallic ball of 0.475 kg was used to impact the centre of the slab. The metallic ball was also not the same as the tire of the aircraft, and could not be used to characterize the impact fatigue of the runway pavement. It was observed that the slabs could sustain a maximum of 130 impact times. Kiran et al. [23] reviewed the impact studies on slabs in the literature. In their review, most of the slab specimens were supported on the four sides or at the four corners, which is different from the supporting condition of the runway pavement. And most of the specimens were seriously damaged after a few impacts, which made it impossible to characterize the impact fatigue behaviour of the runway pavement which may subject to much more number of impacts [21–28].

Although the impact behaviour of the concrete specimens has been widely investigated, the results cannot be directly used to characterize the impact fatigue behaviour of the runway pavement. There are two reasons. Firstly, the impact pressure used in the literature was much higher than the impact pressure of the aircraft on the runway pavement. According to the literature, the maximum vertical ground pressure of Airbus A380 is 1.61 MPa. And the design pressure given in the airfield pavement design standards of China and the United States is in the range of (1.5–2.41 MPa) [20,29,30]. Secondly, the specimens in the literature were mostly supported on the edges or at the corners. However runway pavement should be supported on the underneath basement. Therefore, the impact fatigue behaviour of the runway pavement, especially the proposed GFRP mesh reinforced ECC for runway pavement application, should be specifically investigated.

This paper presents an experimental investigation on the impact fatigue behaviour of the proposed GFRP mesh reinforced ECC runway pavement. The pavement specimens with a dimension of 200 mm × 200 mm × 30 mm (thickness) were prepared and cyclic drop-weight tests were conducted using a specially designed experimental set up [31]. Specimens with one or two layers of GFRP mesh reinforcements were prepared, and the location of the reinforcement in the thickness direction was varied for those specimens with a single layer of mesh. The cyclic impact pressure ranging from 1.61 MPa to 3.60 MPa was applied with a frequency of 23 times/min. The damage pattern and the crack propagation of the specimen were inspected using a portable microscope every 100 impacts. The number of impacts when the first crack appeared and the total impact fatigue life when the specimen completely failed were recorded for each impact pressure. Ultrasonic testing was conducted on damaged specimens and it was proposed as a potential health monitoring method to assess the damage status of the proposed runway pavement.

2. Experimental program

2.1. Materials and mix proportions

The mix proportions of the ECC specimens are presented in Table 1. The raw materials in the mixture of ECC include ordinary Portland cement (P.O 42.5), fly ash, fine aggregate (F-75 silica sand), water, olycarboxylate-based high range water reducing admixture (HRWRA) and the Poly-Vinyl Alcohol (PVA) fibers. The chemical properties of ordinary Portland cement provided by the manufacturer are listed in Table 2. The chemical compositions of fly ash are shown in Table 3. The F-75 silica sand has a maximum grain size of 250 μm and an average grain size of 110 μm. The detailed properties of PVA fibers are summarized in Table 4.

For comparison purpose, the concrete specimens (C) with similar compressive strength to ECC were also prepared based on JGJ 55-2011 [32]. The mix proportion of the concrete is presented in Table 5. The chemical properties of the ordinary Portland cement (P.O 32.5) provided by the manufacturer are listed in Table 2. It should be noted that the cement of P.O 32.5 was used for concrete specimens and the purpose was to prepare concrete specimens with similar compressive strength to ECC. River sand was used in the mixture with a fine modulus of 3.0. The grain size of the coarse aggregate was between 5 mm and 20 mm. Two grid dimensions of 10 mm × 10 mm and 6 mm × 6 mm of GFRP mesh were selected as reinforcements (see Fig. 1). The characteristics of the GFRP mesh provided by the manufacturer are listed in Table 6.

2.2. Sample preparation

The ECC specimens were prepared in a B20 mixer of 20 L capacity. Firstly, the cement, fly ash and silica sand were dry mixed for 5 min at a speed of 168 r/min. Under the same speed, the mixture of water and HRWRA was gradually added and mixed for another 10 min. After that, the PVA fibers were slowly added and mixed for 8 min under the speed of 400 r/min until no fiber agglomeration can be observed. Finally, the mixing was continued for another 2 min until the fibers were well dispersed.

The concrete was prepared in a HJW-60 mixer of 60 L capacity. The cement, sand and stone were dry mixed for 5 min at the speed of 48 r/min and then the water was added and mixed for another 10 min under the same speed.

The GFRP mesh reinforced ECC specimens for the impact fatigue tests had a dimension of 200 mm × 200 mm × 30 mm (thickness). This dimension was selected to accommodate the specially designed digital controlled cyclic impact testing machine which will be introduced in the following discussions. Therefore, GFRP mesh pieces were cut into a size of 200 mm × 200 mm as reinforcements. For specimens with two layers of GFRP mesh reinforcements, the first layer of fresh ECC with a thickness of 10 mm was poured in the mold. Then the first layer of GFRP mesh was put on top of it followed by pouring another 10 mm thick ECC. This process was repeated for the second layer GFRP mesh until the last layer of 10 mm ECC was poured. For specimens with only one layer of GFRP reinforcement, the preparation process was the same except that the GFRP mesh was placed either 10 mm or 20 mm from the top surface of the specimen. The specimens with two layers or one layer of GFRP mesh reinforcements are illustrated in Fig. 2.

In order to achieve the composite action between ECC and GFRP mesh, the fresh ECC was forced to penetrate the holes in the mesh by vibrating the newly made specimens for 3 min on a shaking table. The specimens were demolded after 1 day and cured for another 27 days in air under the temperature of 20 ± 3 °C, and a humidity of 30%±5% RH. The air temperature and humidity were recorded by a digital thermometer and hygrometer (model HTC-1).

In order to characterize the material properties, different types of specimens were prepared for ECC and concrete. Cubic specimens with a dimension of 100 mm × 100 mm × 100 mm were used for the testing of the compressive strength [33]. Dogbone-shaped specimen was prepared for the tensile testing, and the detailed dimensions of it can be found in the recommendations by the Japan Society of Civil Engineers (JSCE) [34].

Table 1
The mixture of ECC.

Water (W) (kg/m^3)	Cement (C) (kg/m^3)	Fly ash (FA) (kg/m^3)	Silica sand (kg/m^3)	PVA fiber		HRWRA kg/m^3	W/(C + FA) Ratio	FA/C Ratio
				By weight (kg/m^3)	By volume (%)			
449	300	950	500	26	2	3.3	0.39	4.7

Table 2
The chemical properties of the ordinary Portland cements (P.O 42.5 and P.O 32.5).

Composition	SiO_2	Al_2O_3	Fe_2O_3	CaO	MgO	C_3S	C_2S	C_3A	C_4AF
P.O 42.5	22.09	5.13	3.79	66.33	1.96	55.62	23.37	6.96	12.39
P.O 32.5	20.33	5.31	4.13	67.21	1.91	57.27	18.31	8.05	12.41

Table 3
The chemical compositions of the fly ash.

Composition	SiO_2	Al_2O_3	Fe_2O_3	CaO	MgO	SO_3	Na_2O	K_2O	Loss on ignition
The fly ash	50.8	28.1	6.2	3.7	1.2	0.8	1.2	0.6	7.9

Table 4
The properties of the PVA fiber.

Diameter (μm)	Length (mm)	Nominal strength (MPa)	Modulus (GPa)	Density (kg/m^3)
40	12	1560	41	1300

Table 5
The mixture of the concrete specimens (kg/m^3).

Cement	Sand	Stone	Water
490	590	1100	220

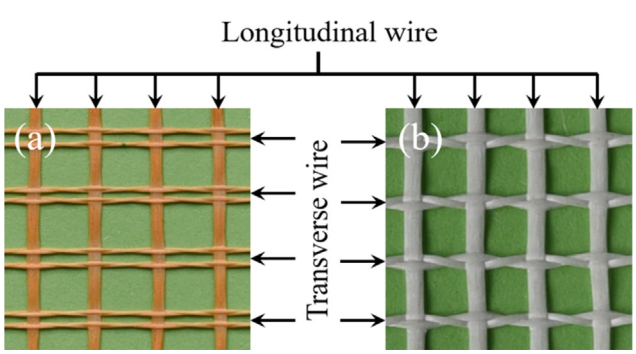

Fig. 1. GFRP mesh (a) M-10, (b) M-6.

2.3. Physical and mechanical testing

The tensile test of ECC was performed using dogbone-shaped specimens according to the JSCE Recommendations [34]. The tests were carried out using a SANS-50kN electronic universal testing machine with displacement control at a speed of 1 mm/min. The tensile experimental set up is shown in Fig. 3.

The compressive strengths of ECC and concrete were determined using three identical 100 × 100 × 100 mm^3 cubic specimens according to GB/T 50081-2002 [33]. The compressive tests were conducted on a WAW-C universal testing machine with a capacity of 2000 kN. The specimens were tested under displacement control at a speed of 1 mm/min. The experimental set up of the compressive testing is shown in Fig. 4.

Tensile tests were conducted according to ISO 4606:1995 [35] to determine the tensile strengths of the GFRP mesh in its two orthotropic directions. The tensile specimen has a gauge length of 100 mm and an unraveled width of 25 mm. SANS-50kN electronic universal testing machine was used to conduct the tensile tests with displacement control at a speed of 1 mm/min. The experimental set up of the GFRP mesh tensile tests is shown in Fig. 5.

Burn-off tests were conducted according to ASTM D 3171-15, in order to determine the fiber content and architecture of the two types of GFRP mesh. A square piece of GFRP mesh with a dimension of 90 mm × 90 mm was cut and placed in a rectangular crucible of 200 mL. The sample was firstly dried in an oven (model BPG-9156A) at 60 °C till the weight of the sample became constant. The dry weight of the sample was recorded as M_m. The weight of another empty crucible was recorded as M_c when cooled down after being heated at 590 °C in a muffle furnace (model KSL-1200X-M). Then the dried GFRP mesh sample was transferred and placed in the second crucible, and heated at 590 °C for 60 min to burn and remove the resin matrix of the mesh. The total weight of the crucible with the GFRP mesh after taken out from the furnace was recorded as M_b. The fiber content of GFRP mesh (f_m) could be calculated by:

$$f_m = \frac{M_m - (M_m + M_c - M_b)}{M_m} \quad (1)$$

2.4. Cyclic impact testing

In order to apply the cyclic impact pressure, a cyclic impact testing machine [31] was specially designed for this study as shown in Fig. 6(a). This machine was modified based on a digital controlled electronic soil compactor (model JDS-1).

Table 6
The characteristics of the GFRP mesh.

ID	Grid dimension (mm × mm)	Weight density (g/m^2)	Tensile strength (N/25 mm width)	
			Transversal	Longitudinal
M-10	10 × 10	125	≥900	≥900
M-6	6 × 6	300	≥2000	≥2000

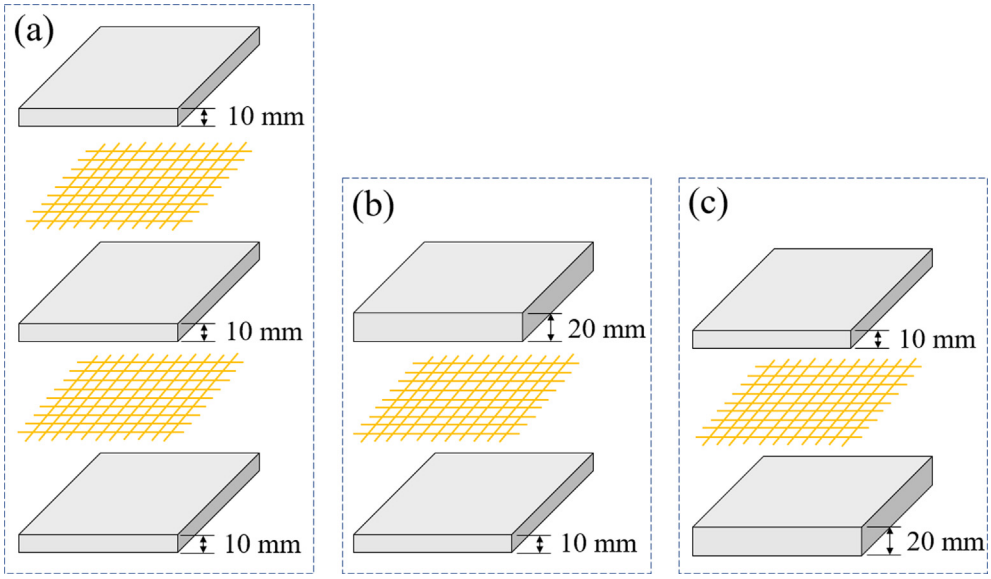

Fig. 2. Illustration of GFRP mesh reinforced ECC specimens with (a) two layers or (b) (c) one layer of GFRP mesh reinforcements.

Fig. 3. The set up of the tensile test of ECC.

Fig. 4. The set up of the compression test.

The impact pressure can be varied by changing the weight of the impact hammer through adding metal weights. The hammer head is in a circular shape with a diameter of 50 mm. To simulate the tires of the airplane, a round industrial rubber with a hardness of 50° and a thickness of 5 mm was glued on the hammer head (see Fig. 6b). The impact frequency was 23 times/min.

A wooden box was fabricated as the container of the specimen and the box was fixed to the ground (see Fig. 6c). A concrete block of 130 mm thick was put inside the wooden box to serve as the foundation of the pavement, which was similar to the work introduced in [22,36,37]. The pavement specimen was put on top of the concrete block. A gap of 3 mm was left between the pavement specimen and the surrounding wooden box to make sure the confinement effect of the wooden box was eliminated.

The impact pressure was firstly calibrated before the cyclic impact testing. The set up for the calibration of the impact pressure is shown in Fig. 7. A force transducer with a capacity of 20 kN (model NOS-F306) was put on top of the concrete block in the wooden box. The upper surface of the force transducer was the same height as that of the pavement specimen. The impact pressure can be recorded when the hammer impacted the transducer. The magnitude of the impact pressure can be changed by adding or removing weights to the hammer.

It was reported that the landing pressure of civilian aircraft and military aircraft could be from 1.2 MPa to 2.41 MPa [20,29,38–41]. For civilian aircraft, the design tire pressure for the runway pavement is 1.5 MPa [20]. For the largest military aircraft, the design tire pressure is 2.41 MPa [29]. It was also reported that the maximum landing tire pressure of A380-800F was 1.61 MPa [41]. In this study, five impact pressures σ were selected, including 1.61 MPa, 1.88 MPa, 2.10 MPa, 2.41 MPa and 3.6 MPa. The first four values cover a representative range of impact pressures by civilian and military aircrafts. The last value is the largest impact pressure that can be applied by the digital controlled cyclic impact machine.

There are 46 airports built in the remote areas of China accounting for 21.1% of the total civilian airports in this country [42]. The cumulative number of aircraft landing times of these remote airports was less than 27,000 times within their design life of 30 years [43]. Therefore, a maximum number of impact times of 30,000 was selected in this study to represent the pavement design of most remote

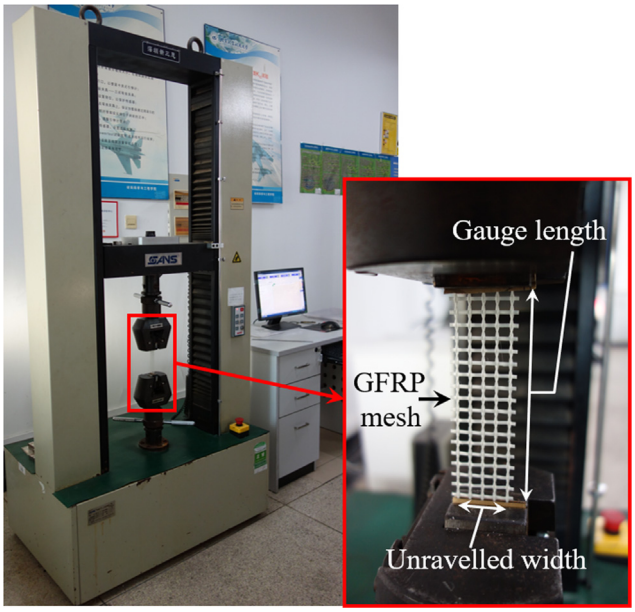

Fig. 5. The set up of the tensile test of GFRP mesh.

airports, and at the same time saving experimental time. Actually, the aircrafts may not always land on the same point of the runway in the field. In the current experimental program, the impact was applied at the same point of pavement specimen for upto 30,000 times. Therefore, the experimental condition can be considered as the most severe impact condition in the field and thus the results can be conservative.

In the experimental setup in Fig. 6, the ECC pavement was placed on top of a concrete block which was fixed to the basement. This setup was to simulate the field application when ECC is a surface layer of a multiple layer runway pavement system. This setup has been adopted by a number of research [22,23] in the literature on the impact behaviour of concrete pavement. Although this setup cannot represent exactly the same field conditions, it can be considered as reliable to provide fundamental understanding on the impact behaviour of pavement. These preliminary understandings become particularly valuable especially when there is limited research in the literature on this issue.

2.5. Ultrasonic testing

The cyclic impact pressure would incur cumulative damages to the runway pavement which is often difficult to be quantified. It is necessary to develop a method to characterize the damage accumulation so that the service life of different pavement materials can be compared. At the same time the in-field health assessment of the runway pavement can be made possible using this damage characterization method. In this paper, an ultrasonic testing method [43], which is a routine technology in the structural health monitoring field [44–49] and convenient to set up in the laboratory scale, is resorted to characterize he damage accumulation behaviour of the proposed GFRP mesh reinforced ECC for runway pavement application.

The test set up in Fig. 8 consists of a pulse generator (model 5577PR), an oscilloscope (model DPO2014), and two acoustic sensors (model P28F-50K). One sensor was used as transmitting transducer and the other one was used as receiving transducer. The pulse generator and the transmitting transducer could generate voltage pulses. After the pulses of voltage traversing through the specimen, the pulses are received and converted into electric energy by the receiving transducer. The transit time (T) is measured electronically. The pulse velocity V could be calculated by dividing the distance between the transmitting and receiving transducers, L (which is equal to the length of specimens: 200 mm) by the transit time T. The lower the pulse velocity is, the more damages the specimen would have. By correlating the pulse velocity, the impact pressure, and the number of impact times, it will be possible to develop a damage assessment algorithm for the runway pavement subjected to cyclic impact pressure.

3. Experimental results and discussions

3.1. Physical and mechanical testing

The 28-day compressive strengths of ECC and concrete were 31.5 MPa and 33.0 MPa, respectively. The tensile strain hardening behaviour of ECC can be clearly observed in its stress strain curve in Fig. 9. The ultimate tensile strain of ECC in this study was 3.2%, and the tensile specimen exhibited multi cracking behaviour as shown in Fig. 9.

For GFRP mesh, the average tensile strength of three identical specimens was 1204.94 N/25 mm-width for the mesh with 6 mm grid (M-6) and 504.07 N/25 mm-width for M-10 in the longitudinal direction. Similarly the tensile strength in the transverse direction was 1205.55 N/25 mm-width and 506.34 N/25 mm-width for M-6 and M-10, respectively.

The fiber architecture and fiber content were analyzed using burn-off tests with three identical samples and the testing procedure was described in Section 2.3. The average fiber content of M-6 was 87.6% with a standard deviation 0.46%, and the average fiber content of M-10 was 87.3% with a standard deviation of 0.53%. The two types of GFRP mesh before and after the burn-off test are shown in Fig. 10 with detailed fiber architecture and configuration at the joint location.

3.2. Cyclic impact testing

As introduced in Section 2.4, five impact pressures σ were selected in this study i.e. 1.61 MPa, 1.88 MPa, 2.10 MPa, 2.41 MPa and 3.60 MPa which cover a reasonable range of the impact pressure applied by commercial and military aircrafts on the runway pavement. For each selected impact pressure, the test stopped when the specimen completely failed or the maximum impact number of 300×10^2 times was reached. The complete failure of the specimen was determined when any crack penetrated the entire thickness of the specimen.

For each test, the specimen was inspected every 100 impact times using a crack detector (model KON-FK(B)). When the first crack appeared, the number of impact times was recorded and denoted as the impact fatigue life N_0. Similarly, the total number of impact times was also recorded and represented with N_C corresponding to the complete failure of the specimen.

A total number of 22 specimens were tested under cyclic impact pressure as listed in Table 7. The last number of the specimen ID in Table 7 represents the applied impact pressure with a unit of MPa. For comparison purpose, concrete specimen "C" with similar compressive strength as ECC was tested. "ECC" specimen has no GFRP reinforcements. "EM-6 × 2" has two layers of M-6 mesh located 10 mm and 20 mm from the top surface of the specimen (total thickness of 30 mm, see Fig. 2a). "EM-10 × 2" is the same as "EM-6 × 2" except that the two layers mesh are M-10. "EM-10 × 1-top" and "EM-10 × 1-bot" are specimens with only one layer of M-10 mesh at different locations, i.e. 10 mm and 20 mm from the top surface of specimen respectively (see Fig. 2b and c). These two specimens were only tested under the impact pressure of 1.61 MPa, in order to study the effect of mesh location on the cyclic impact behaviour of GFRP mesh reinforced ECC pavement.

3.2.1. Effect of σ on N_0 at the first crack of specimen

The impact fatigue lives N_0 at the first crack of specimens C, ECC, EM-6 × 2 and EM-10 × 2 are plotted against the corresponding impact pressures σ in Fig. 11. This plot has a similar concept to the S-N curve in the fatigue design of steel structures. It is obvious that, for each type of specimen, N_0 increases with the decrease of σ. Concrete specimen C showed very poor cyclic impact behaviour, and the first crack occurred only after several impacts. For example, N_0 of concrete specimen was only 3, 4, 5, 7, 10 under the corresponding σ of 3.60 MPa, 2.41 MPa, 2.10 MPa, 1.88 MPa, 1.61 MPa respectively. On the other hand, ECC specimens exhibited much better cyclic impact performance especially when reinforced with GFRP mesh. For example, N_0 of ECC without reinforcement increased from 4×10^2 to 10×10^2, 21×10^2, 38×10^2, 50×10^2

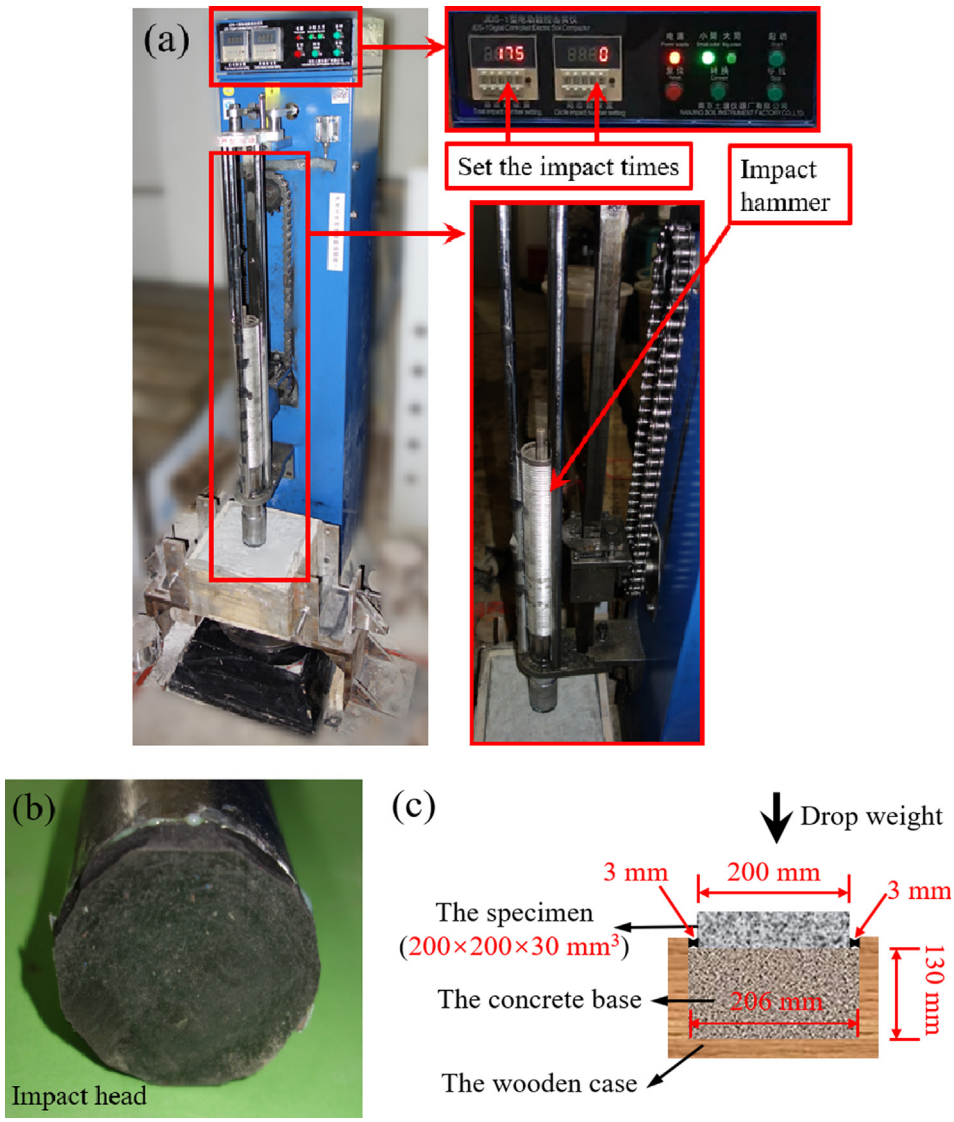

Fig. 6. The set up of the cyclic impact test (a) the digital controlled electronic soil compactor, (b) the impact head, and (c) the concrete base and the wooden case.

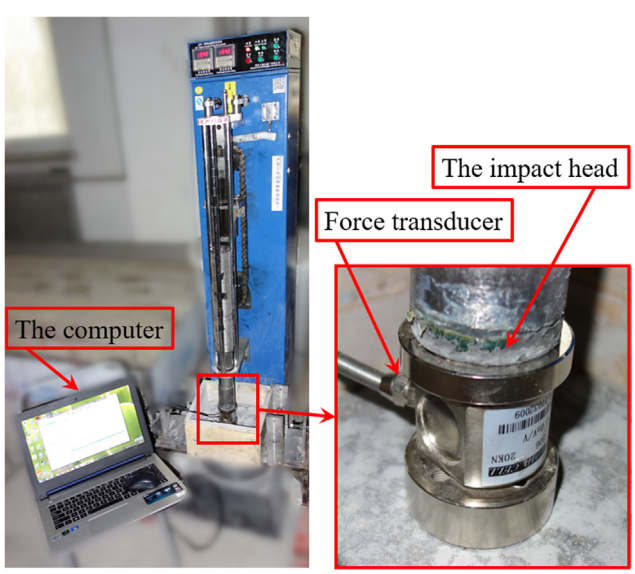

Fig. 7. The set up for the calibration of the impact pressure.

times when σ gradually decreased from 3.60 MPa to 1.61 MPa. When two layers of GFRP mesh with 6 mm grid were used as reinforcements, EM-6 × 2 had improved N_0 i.e. increasing from 7×10^2 to 78×10^2 with σ decreased from 3.60 MPa to 1.61 MPa. The highest N_0 was achieved by ECC with two layers of M-10 mesh reinforcements (specimen EM-10 × 2). For example, N_0 of EM-10 × 2 was 9×10^2, 22×10^2, 50×10^2, 78×10^2, 106×10^2 under the corresponding σ of 3.60 MPa, 2.41 MPa, 2.10 MPa, 1.88 MPa, 1.61 MPa respectively.

When comparing N_0 of different specimens at the same σ, the cyclic impact performance follows the order of EM-10 × 2>EM-6 × 2>ECC≫C. For example, under 1.61 MPa, the first crack of concrete specimen C was observed only after 10 impacts. ECC showed an extensive improvement in N_0 (50×10^2) with an increasing ratio of 500 when normalized with N_0 of C. When two layers of M-6 were used as reinforcements of ECC, N_0 was 78×10^2. The best cyclic impact behaviour was achieved when ECC was reinforced with two layers of M-10 ($N_0 = 106 \times 10^2$). Similarly, at the highest impact pressure of 3.60 MPa, N_0 still followed the order of EM-10 × 2 (9×10^2)>EM-6 × 2 (7×10^2)>ECC (4×10^2)≫C (3).

When N_0 of other types of specimens are normalized by N_0 of C, and the ratios at the five impact pressures are averaged for one

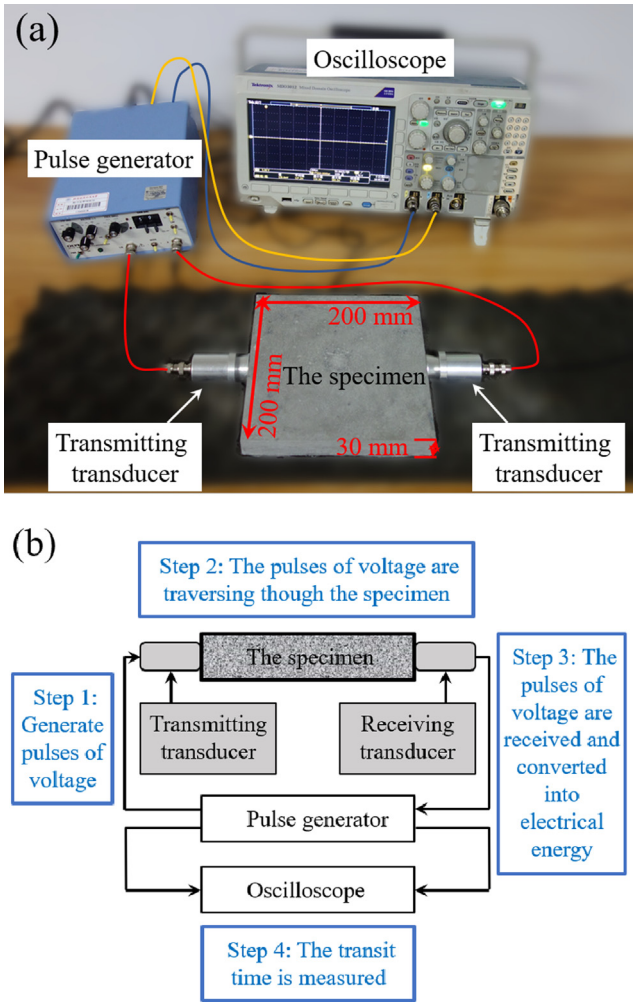

Fig. 8. (a) The set up of the ultrasonic test, and (b) the brief schematic diagram of the ultrasonic test.

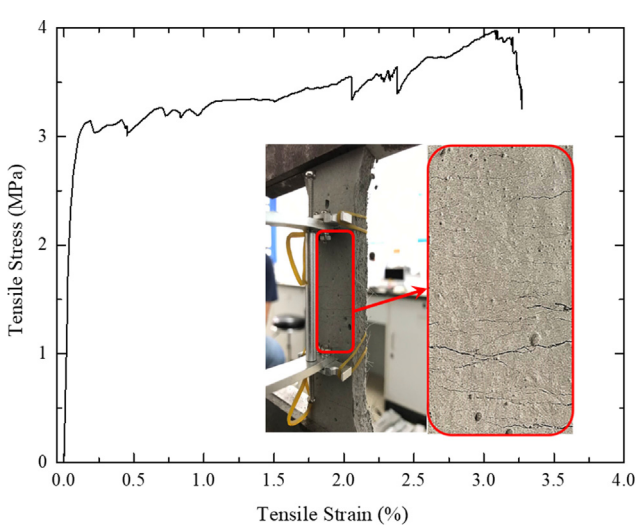

Fig. 9. The tensile stress–strain curve of ECC.

specific type of specimen, it can be found that N_0 is improved by 369.2, 545.2 and 804.8 times for ECC, EM-6 × 2 and EM-10 × 2 respectively when comparing with concrete specimen C. Similarly, when ECC was reinforced with two layers of M-6 and M-10, N_0 was improved by 1.5 and 2.2 times on average respectively when comparing with that of ECC without reinforcements.

3.2.2. Effect of σ on N_C at the complete failure of specimen

The total impact fatigue lives N_C at the complete failure of specimens C, ECC, EM-6 × 2 and EM-10 × 2 are plotted against the corresponding σ in Fig. 12. For concrete specimens, N_C is the same as N_0 because concrete is brittle and completely failed as soon as the first crack appeared. ECC exhibited complete failure only under two impact pressures of 2.41 MPa and 3.60 MPa and the corresponding N_C were 210×10^2 and 169×10^2, respectively. ECC specimens with GFRP mesh reinforcements (EM-6 × 2 and EM-10 × 2) did not completely fail after 300×10^2 impact times regardless of the applied σ.

The ECC specimens with complete failure (ECC-2.41 and ECC-3.60) are presented in Fig. 13 with photos showing the cracking at the bottom and side of the specimens. The failure mode of concrete specimen is also included in Fig. 13 for comparison. The rough region at the center of the bottom surface of ECC specimens was generated by the friction of specimen with the underneath concrete block (Fig. 13) during the impact testing. It is obvious from the bottom surface photos in Fig. 13 that ECC specimens developed a number of microcracking before complete failure whereas concrete specimens failed due to macrocracks under cyclic impact pressure.

The photos showing the bottom surface of all specimens after the completion of all tests are compared in Fig. 14. The type of specimens are listed on the left of Fig. 14 with the values on top denoting the corresponding cyclic impact pressures. The number in each photo represents the corresponding impact fatigue life at the complete failure of specimen. The micro cracks on ECC specimens are marked with white lines for better identification. A red circle of 150 mm in diameter is drawn in the center of each photo in order to assist the observation of the extension of the micro cracks. It is obvious in Fig. 14 that concrete specimens failed immediately after the macro cracks occurred. For ECC specimens with/without GFRP mesh reinforcements, micro cracks were developed and more micro cracks extended beyond the red circle with the increase of cyclic impact pressures.

3.2.3. Effect of GFRP mesh location on the cyclic impact behaviour of specimens

Two specimens EM-10 × 1-top and EM-10 × 1-bot were prepared which were reinforced with one layer of M-10. The difference between these two specimens is the location of the M-10 mesh (see Fig. 2), i.e. EM-10 × 1-top has the mesh embedded 10 mm underneath the top surface whereas EM-10 × 1-bot has the mesh located 20 mm from the top surface (impact surface). These two specimens were tested under cyclic impact pressure of 1.61 MPa. By comparing the results of these two specimens, the effect of mesh location on the impact fatigue behaviour of GFRP mesh reinforced ECC can be studied.

Similar to the specimens ECC and EM-10 × 2, specimens EM-10 × 1-top and EM-10 × 1-bot did not completely fail under 1.61 MPa after 300×10^2 times of cyclic pressure. The impact fatigue lives N_0 when the first crack appeared for specimens ECC, EM-10 × 2, EM-10 × 1-top and EM-10 × 1-bot are compared in Fig. 15. It is clear in Fig. 15 that, N_0 increased from 56×10^2 to 82×10^2 cycles with an improvement of 46.4% when the one layer of M-10 mesh was moved from top (EM-10 × 1-top) to the bottom of specimen (EM-10 × 1-bot). This observation indicates that GFRP mesh is effective in resisting cyclic impact pressure when the mesh is in tension. If the mesh reinforcement is placed on top of the specimen, the mesh would be in compression and its contribution on N_0 is minimal. For example, N_0 of EM-10 × 1-top (56×10^2) is very similar to that of to ECC without reinforcement

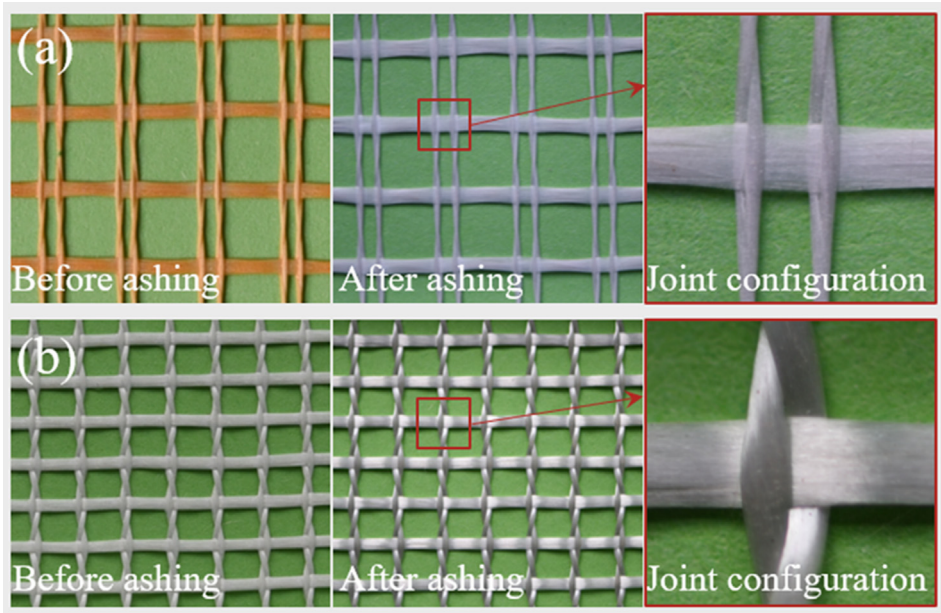

Fig. 10. Images of two types of GFRP mesh (a) M-10 and (b) M-6 before and after burn-off tests with detailed fiber architecture and configuration at the joint location.

Table 7
The specimens tested under various cyclic impact pressures.

Specimen ID		Mesh	Mesh location from top surface of specimen	N_0	N_C
1	C-1.61	No	N/A	10	10
2	C-1.88			7	7
3	C-2.10			5	5
4	C-2.41			4	4
5	C-3.60			3	3
6	ECC-1.61	No	N/A	5000	30,000
7	ECC-1.88			3800	30,000
8	ECC-2.10			2100	30,000
9	ECC-2.41			1000	16,900
10	ECC-3.60			400	21,000
11	EM-6 × 2–1.61	2 layers of M-6	10 mm and 20 mm	7800	30,000
12	EM-6 × 2–1.88			5200	30,000
13	EM-6 × 2–2.10			2600	30,000
14	EM-6 × 2–2.41			1800	30,000
15	EM-6 × 2–3.60			700	30,000
16	EM-10 × 2–1.61	2 layers of M-10	10 mm and 20 mm	10,600	30,000
17	EM-10 × 2–1.88			7800	30,000
18	EM-10 × 2–2.10			5000	30,000
19	EM-10 × 2–2.41			2200	30,000
20	EM-10 × 2–3.60			900	30,000
21	EM-10 × 1-top-1.61	1 layer of M-10	10 mm	5600	30,000
22	EM-10 × 1-bot-1.61	1 layer of M-10	20 mm	8200	30,000

($N_0 = 50 \times 10^2$) showing only 12% increase. The best impact fatigue behaviour was achieved by EM-10 × 2 with $N_0 = 106 \times 10^2$ showing an improvement by 112% comparing to ECC. This suggests that it is always helpful to place two layers of mesh reinforcements in ECC and if it is not applicable, the mesh reinforcement should be placed at the bottom of the specimen (tension side) to resist the cyclic impact pressure.

The cracking patterns of the bottom surfaces of specimens ECC, EM-10 × 1-top, EM-10 × 1-bot and EM-10 × 2 after 300×10^2 cyclic impact pressure are compared in Fig. 16. A red circle with a diameter of 150 mm is drawn in the center of each specimen. It is obvious in Fig. 16 that, the cracks of specimens ECC and EM-10 × 1-top extended beyond the red circle while the cracks of specimens EM-10 × 1-bot and EM-10 × 2 are shorter and confined within the circular region. Also, EM-10 × 2 showed less and shorter cracks comparing to EM-10 × 1-bot. These observations comply with the N_0 results in Fig. 16, which is EM-10 × 2>EM-10 × 1-bot>EM-10 × 1-top≈ECC in terms of impact fatigue performance.

3.3. Damage accumulation assessment using ultrasonic testing

It can be seen in Fig. 14 that normal concrete fails immediately when macro cracks appears, whereas GFRP mesh reinforced ECC specimens develops considerable number of micro cracks before complete failure. This indicates that the damage condition of normal concrete pavement can be conveniently identified by visual inspections. However, the damage status of ECC pavement is difficult to determine regardless of the inclusion of GFRP mesh rein-

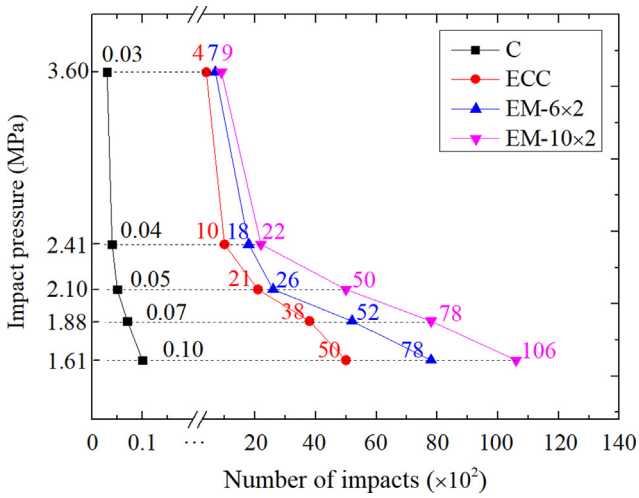

Fig. 11. Effect of σ on N_0 of C, ECC, EM-6 × 2 and EM-10 × 2.

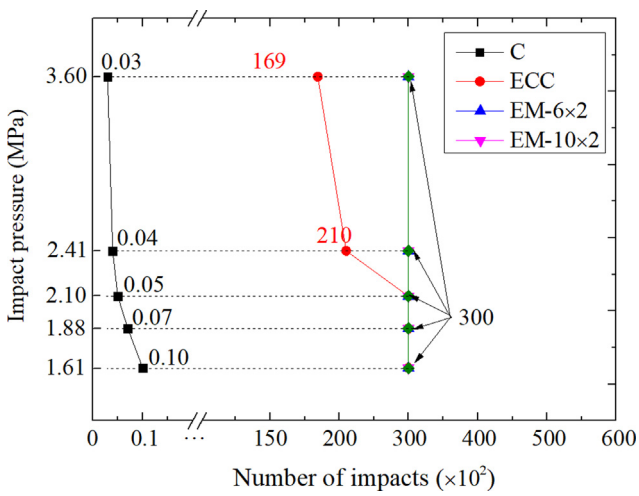

Fig. 12. Effect of σ on N_C of C, ECC, EM-6 × 2 and EM-10 × 2.

forcement or not. The top surface of GFRP mesh reinforced ECC pavement may look intact but with extensive damages accumulate inside. Therefore, it will be very helpful to develop a non destructive method to assess the damage accumulation of the pavement. In this paper, the routine technique used in structural health monitoring through ultrasonic testing is proposed. The detailed ultrasonic testing scheme is introduced in Section 2.5.

The progressive development of the micro cracks of specimens EM-6 × 2 and EM-10 × 2 under various impact pressures were recorded using a camera every 50 × 10^2 impacts and the examples under 1.61 MPa are shown in Fig. 17. The numbers on top of Fig. 17 indicate the number of impacts when the photo was taken. It is clear that more micro cracks were developed and these cracks became longer with the increased number of impacts, indicating the accumulation of damages.

In order to quantify the damage accumulations in GFRP mesh reinforced ECC specimens, the pulse velocity (V) through each specimen was recorded every 50 × 10^2 impacts. The details on how to measure V was introduced in the ultrasonic testing scheme in Section 2.5. In the following discussions, V_0 denotes the pulse velocity of a specimen before the cyclic impact test and V_N means the pulse velocity of the same specimen after N times of impacts. The ratio $\alpha = V_N/V_0$ is plotted against N in Fig. 18 for EM-6 × 2 and EM-10 × 2 specimens under various cyclic impact pressures.

Several observations can be made in Fig. 18. Firstly, for all specimens, α gradually decreased with the increased number of impacts. This means the pulse velocity V_N became smaller indicating more damages developed within the specimen with the continuous application of cyclic impacting. Secondly, at the same N, α decreased with the increase of impact pressures. This indicates higher impact pressure would generate more damages in specimens. For example, at N = 300 × 10^2, α of EM-10 × 2 decreased from 0.928 to 0.834 when the impact pressure increased from 1.61 MPa to 3.6 MPa showing a 10.1% reduction. Finally, under the same impact pressure, the descending trend of α for EM-6 × 2 is faster than that of EM-10 × 2. This suggests that GFRP mesh reinforcements are helpful to improve the cyclic impact behaviour of ECC, especially when M-10 mesh is used. These obser-

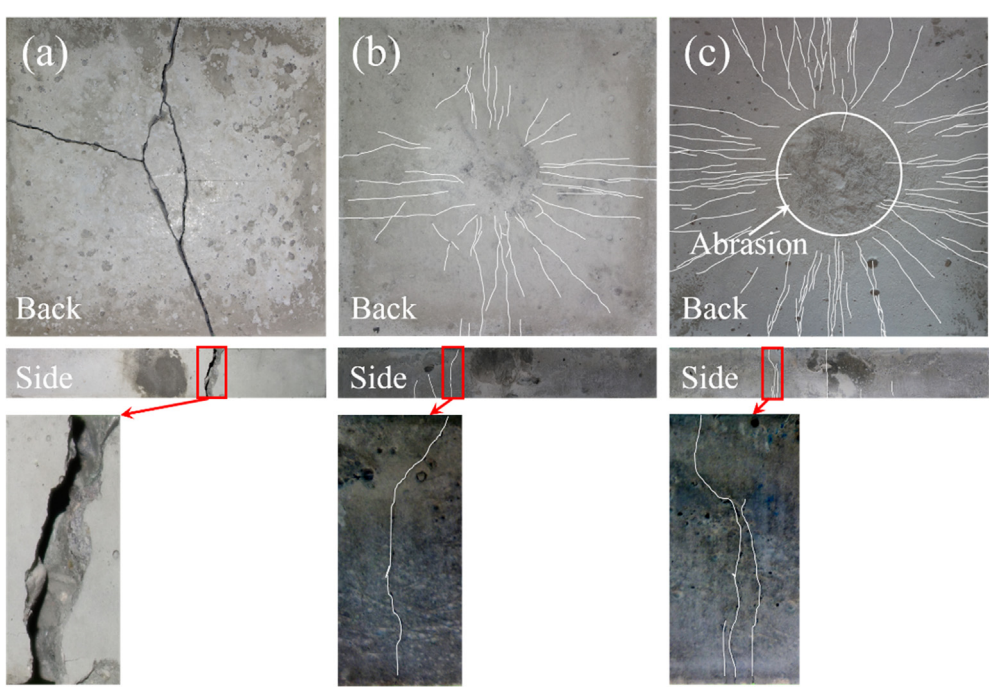

Fig. 13. The complete failure mode of (a) concrete, and ECC specimens under the impact pressure of (b) 2.41 MPa and (c) 3.60 MPa.

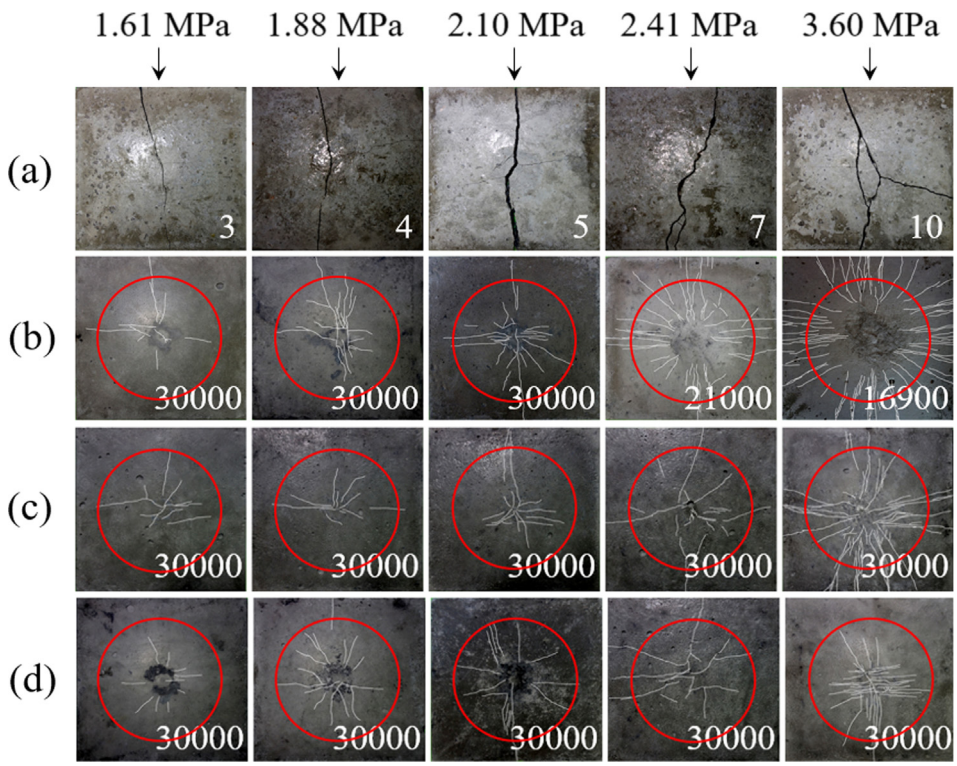

Fig. 14. Cracking pattern on the bottom surfaces of (a) C, (b) ECC, (c) EM-6 × 2, and (d) EM-10 × 2 at the completion of the tests.

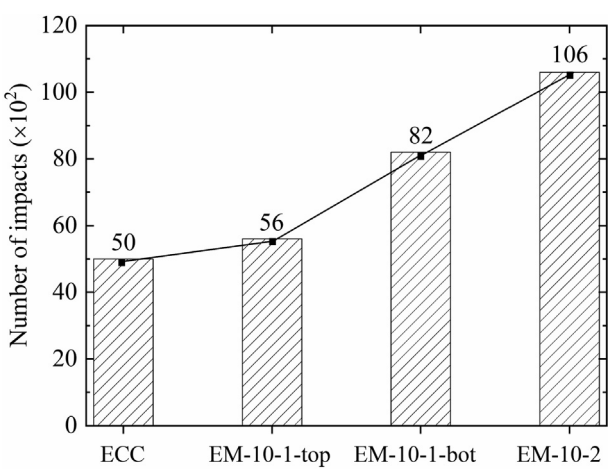

Fig. 15. N_0 of specimens ECC, EM-10 × 1-top, EM-10 × 1-bot and EM-10 × 2 under cyclic impact pressure of 1.61 MPa.

vations in Fig. 18 well comply with the experimental observations in Fig. 17.

It can be seen in Fig. 18 that, α is almost linearly related to N for GFRP mesh reinforced ECC specimens. A group of linear fitting lines are also plotted in Fig. 18. The descending slop of these α-N lines is defined as K, so that the linear relationship between α and N can be expressed as

$$\alpha = -KN + 1 \text{ where } \alpha = V_N/V_0 \tag{2}$$

It is clear in Fig. 18 that, for EM-6 × 2 and EM-10 × 2, K is dependent on the corresponding impact pressure. The values of K are plotted against the corresponding impact pressures in Fig. 19 for EM-6 × 2 and EM-10 × 2 specimens (coefficient of determination of Equation (3.1) and (3.2) are 0.87396 and 0.98249, respectively). It is interesting to see in Fig. 19 that, K is generally linear related to σ. And the linear fitting lines (Eq. 3) for EM-6 × 2 and EM-10 × 2 are parallel to each other.

$$K = 1.8 \times 10^{-6}\sigma + 6.0 \times 10^{-7} \quad \text{for EM - 6} \times 2 \tag{3.1}$$

$$K = 1.8 \times 10^{-6}\sigma - 4.8 \times 10^{-7} \quad \text{for EM - 10} \times 2 \tag{3.2}$$

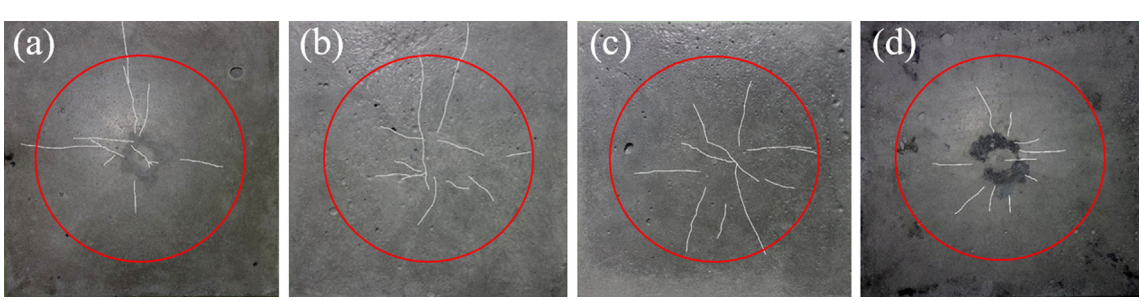

Fig. 16. Cracking pattern at the bottom surfaces of (a) ECC, (b) EM-10 × 1-top, (c) EM-10 × 1-bot and (d) EM-10 × 2 after 300 × 10^2 cyclic impact pressure of 1.61 MPa.

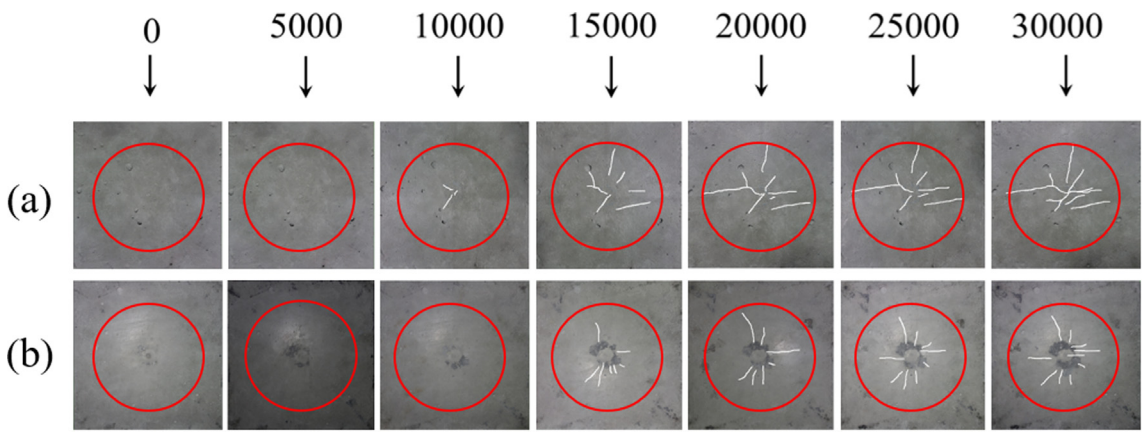

Fig. 17. Progressive crack development on the bottom surfaces of (a) EM-6 × 2 and (b) EM-10 × 2 under the impact pressure of 1.61 MPa.

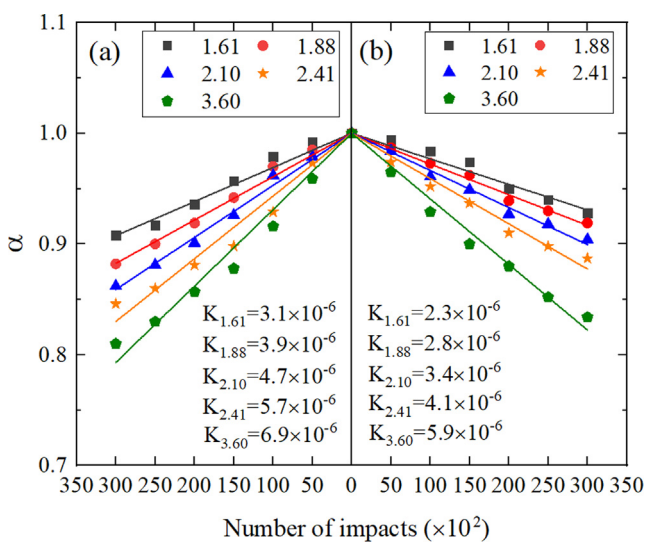

Fig. 18. The relationship between the ratio $\alpha = V_N/V_0$ and number of impacts N for (a) EM-6 × 2 and (b) EM-10 × 2 specimens under various impact pressures.

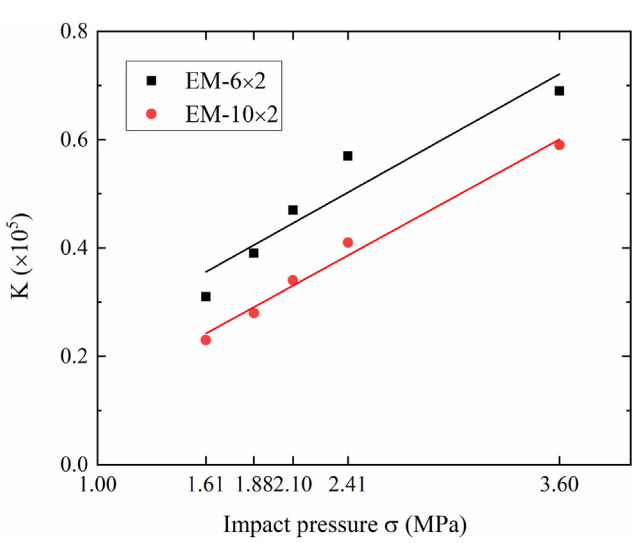

Fig. 19. The relationship between K and impact pressure σ for EM-6 × 2 and EM-10 × 2 specimens.

By combining Eqs. (2) and (3), the pulse velocity V_N can be expressed as:

$$\alpha = -f(\sigma)N + 1 \text{ where } \alpha = V_N/V_0 \tag{4}$$

Eq. (4) is proposed as a theoretical model to assess the damage status of GFRP reinforced ECC specimens. According to Eq. (4), α, as a function of N and σ, should be a curved surface in the coordinate system of (α, N, σ). The theoretical α is plotted against the experimental α data in Fig. 20 for comparison purpose. It can be seen that the proposed theoretical model of α agreed well with the experimental results.

As mentioned in Section 2.4, the design impact fatigue life of the runway pavement of most remote airports is around 300×10^2 impacts. By using Eq. (4), the remaining impact fatigue life of the runway pavement can be predicted by the following steps: (1) The pulse velocity V_0 is measured of the intact specimen before being subjected to cyclic impact pressure; (2) Under a specific impact pressure σ, the pulse velocity V_N is recorded after a period of service time; (3) Substitute σ, V_0 and V_N in Eq. (4), and the corresponding N can be determined, and the remaining fatigue life should be 300×10^2-N. Therefore, Eq. (4) can serve as a quantitative method to assess the damage status and determine the remaining impact fatigue life of the proposed GFRP mesh reinforced ECC pavement.

4. Conclusions

This paper investigated the impact fatigue behaviour of the GFRP mesh reinforced ECC for runway pavement application under the design aircraft pressure. Compared with the previous studies, the service life could be analysed directly in this research. Cyclic impact tests were conducted and the number of impacts when the first crack occurred and the number of impacts at the complete failure were reported. A health monitoring algorithm based on the ultrasonic testing method was proposed to assess the damage status and predict the remaining cyclic impact fatigue life the pavement. Based on the research of this study, the following conclusions could be drawn:

(1) The concrete pavement specimens failed after only several impacts due to macro cracks, while GFRP mesh reinforced ECC pavement specimens could sustain 30,000 impacts with the development of micro cracks without failure.
(2) GFRP mesh is helpful to improve the cyclic impact fatigue behaviour of the GFRP mesh reinforced ECC pavement, especially when the mesh with larger grade size is used as reinforcements.

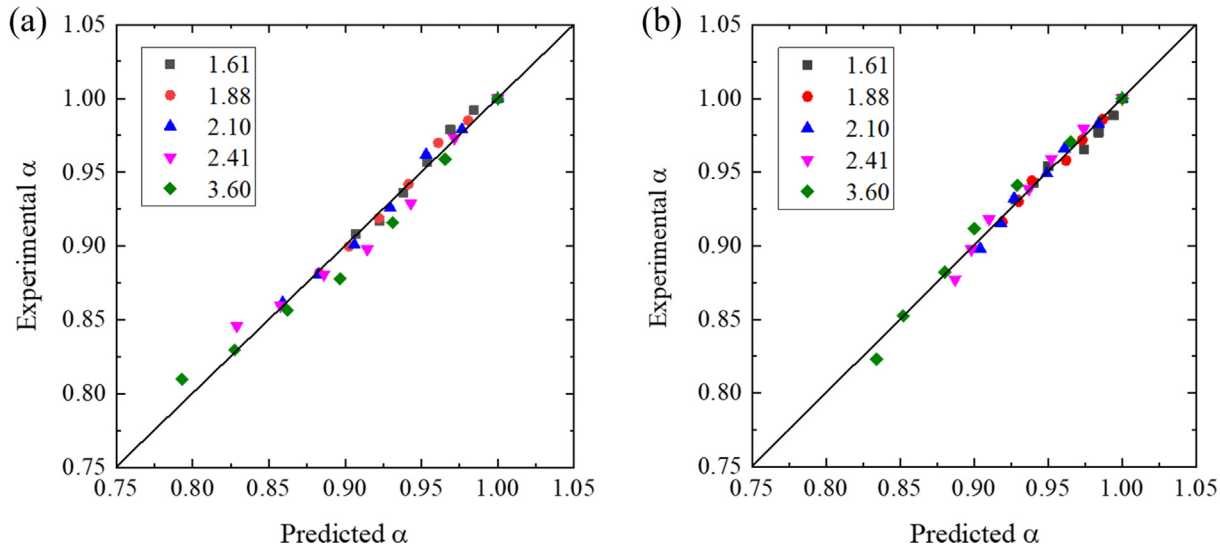

Fig. 20. Comparison between the predicted and experimental α for (a) EM-6 × 2 and (c) EM-10 × 2.

(3) It is recommended that GFRP mesh to be placed at the bottom of the pavement, so that the mesh is in tension when the impact is applied on the top surface of the pavement. The effect of the GFRP mesh reinforcement is minimal when place on top of the pavement. Whenever possible, it is better to place two layers of GFRP mesh reinforcements in the ECC pavement.
(4) The proposed non-destructive health monitoring algorithm based on ultrasonic testing method is helpful to assess the damage status of the GFRP mesh reinforced ECC pavement and predict its remaining cyclic impact fatigue life.

Generally, the proposed GFRP mesh reinforced ECC pavement satisfies the requirements of airports built in remote regions. This is because the pavement could sustain at least 30,000 impacts considering the impact pressures adopted in this paper, which corresponds to 30 years of service life of the pavement. It is recommended that the durability behaviour of this pavement to be further studied when subjected to various environmental conditions before it can be safely used in field applications.

The aim of this research is to understand the applicability of the proposed GFRP mesh reinforced ECC system for airport runway pavement from the perspective of impact behaviour. The results presented in this paper are based on the setup in laboratory conditions. Although this experimental setup and method have been used by many researchers in the literature [22,23] to study the behaviour of concrete pavement and therefore can be considered as reliable, they cannot represent exactly the same field conditions. Considering the fact that there is limited study on ECC runway pavement applications from the perspective of impact behaviour, the study presented in this paper contributes to the preliminary understanding on the impact behaviour of GFRP mesh reinforced ECC when used as a pavement material or as a surface repair material of concrete pavement for airport runway applications.

Acknowledgements

The authors gratefully acknowledge the financial support provided by the National Science Foundation of China (51608020, 51911530208, 51978025). This work was also funded by the Thousand Talents Plan (Young Professionals) in China.

Declaration of Competing Interest

The authors declare that they have no known competing financial interests or personal relationships that could have appeared to influence the work reported in this paper.

References

[1] I. Ahmed, M. Rahman, S. Seraj, A. Hoque, Performance of plain concrete runway pavement, J. Perform. Constr. Facil. 12 (3) (1998) 145–152.
[2] K.D. Smith, J.R. Roesler, Review of fatigue models for concrete airfield pavement design, Airfield Pavements: Challenges and New Technologies, 2004, pp. 231–258.
[3] F. Giussani, F. Mola, Durable concrete pavements: the reconstruction of runway head 36R of Milano Linate International Airport, Constr. Build. Mater. 34 (3) (2012) 352–361.
[4] J. Yang, G. Jiang, Experimental study on properties of pervious concrete pavement materials, Cem. Concr. Res. 33 (3) (2003) 381–386.
[5] M. Fakhri, R.S. Dezfoulian, A. Golroo, B. Makkiabadi, Developing an approach for measuring the intensity of cracking based on geospatial analysis using GIS and automated data collection system, Int. J. Pavement Eng. 6 (2019) 1–15.
[6] R. Hussin, N. Ismail, S. Mustapa, A study of foreign object damage (FOD) and prevention method at the airport and aircraft maintenance area, IOP Conf. Ser. Mater. Sci. Eng. 152 (1) (2016) 012038–012048.
[7] Department of Defence. Airfield Pavement Maintenance Manual, Beca Consultants Pty Ltd, Victoria, 2015.
[8] I.T. Roh, K.C. Jung, S.H. Chang, Y.H. Cho, Characterization of compliant polymer concretes for rapid repair of runways, Constr. Build. Mater. 78 (2015) 77–84.
[9] J. Zhang, X. Weng, B. Yang, Y. Li, J. Liu, L. Jiang, Bonding characteristics of grouting layer in prefabricated cement concrete pavement, Constr. Build. Mater. 145 (2017) 528–537.
[10] T. Guo, Y. Xie, X. Weng, Evaluation of the bond strength of a novel concrete for rapid patch repair of pavements, Constr. Build. Mater. 186 (2018) 790–800.
[11] V.C. Li, Tailoring ECC for special attributes: a review, Int. J. Concr. Struct. Mater. 6 (3) (2012) 135–144.
[12] Z. Pan, C. Wu, J. Liu, W. Wang, J. Liu, Study on mechanical properties of cost-effective polyvinyl alcohol engineered cementitious composites (PVA-ECC), Constr. Build. Mater. 78 (2015) 397–404.
[13] K. Yu, L. Li, J. Yu, Y. Wang, J. Ye, Q.F. Xu, Direct tensile properties of engineered cementitious composites: a review, Constr. Build. Mater. 165 (2018) 346–362.
[14] S. Wang, A.E. Naaman, V.C. Li, Bending response of hybrid ferrocement plates with meshes and fibers, J. Ferrocement 34 (1) (2004) 275–288.
[15] N. Gattesco, I. Boem, Experimental and analytical study to evaluate the effectiveness of an in-plane reinforcement for masonry walls using GFRP meshes, Constr. Build. Mater. 88 (2015) 94–104.
[16] A.V. Oskouei, A. Jafari, M. Bazli, R. Ghahri, Effect of different retrofitting techniques on in-plane behavior of masonry wallettes, Constr. Build. Mater. 169 (2018) 578–590.
[17] M. Tsesarsky, A. Peled, A. Katz, I. Anteby, Strengthening concrete elements by confinement within textile reinforced concrete (TRC) shells – Static and impact properties, Constr. Build. Mater. 44 (44) (2013) 514–523.
[18] T. Triantafillou, Textile Fibre Composites in Civil Engineering, Elsevier Ltd., Duxford, 2016.

[19] A. Borri, G. Castori, M. Corradi, R. Sisti, Masonry wall panels with GFRP and steel-cord strengthening subjected to cyclic shear: An experimental study, Constr. Build. Mater. 56 (2014) 63–73.
[20] MH/T5004-2010. Specifications for airport cement concrete pavement design, 2010.
[21] R. Ranade, V.C. Li, W.F. Heard, B.A. Williams, Impact resistance of high strength-high ductility concrete, Cem. Concr. Res. 98 (2017) 24–35.
[22] J. Wu, X. Liu, C. Zhang, Experimental study on multi-layer composite pavement system under drop weight impacts. Mechanics of Structures and Materials: Advancements and Challenges, Proceedings of the 24th Australian Conference on the Mechanics of Structures and Materials, 1, CRC Press, Balkema, 2017, pp. 861–866.
[23] T. Kiran, A.M. Arjun, A.K.Z. Sadath, Impact analysis on slabs-a review, Int. Res. J. Eng. Technol. 4 (5) (2017) 423–426.
[24] G. Ramakrishna, T. Sundararajan, Impact strength of a few natural fibre reinforced cement mortar slabs: a comparative study, Cem. Concr. Compos. 27 (5) (2005) 547–553.
[25] K.C.G. Ong, M. Basheerkhan, P. Paramasivam, Resistance of fibre concrete slabs to low velocity projectile impact, Concr. Concr. Compos. 21 (1999) 391–401.
[26] Y. Chen, I.M. May, Reinforced concrete members under drop-weight impacts, Proc. Inst. Civil Eng. Struct. Build. 162 (2009) 45–56.
[27] S.H. Rao, V.G. Ghorpade, N.V. Ramana, K. Gnaneswar, Response of SIFCON two-way slabs under impact loading, Int. J. Impact Eng. 37 (2010) 452–458.
[28] S. Elavenil, G.M.S. Knight, Impact response of plates under drop weight impact testing, Int. Univ. J. Sci. Technol. 7 (2012) 1–11.
[29] MIL-HDBK-1021/2. Military handbook general concepts for airfield pavement design, 1973.
[30] R. Cojocaru, J.C. Pais, A. Radu, M. Budescu, Modelling of airport rigid pavement structure made of RCC and recycled cement concrete for complex configuration of landing gears, Adv. Mater. Res. 649 (2013) 254–257.
[31] J.S. Zhang, W.M. Zhang, A new equipment and the test method for the impact fatigue test of the concrete, CN201711235189.2, China, 2017.
[32] JGJ 55-2011. Specification for mix proportion design of ordinary concrete, 2011.
[33] GB/T 50081-2002. Standard for test method of mechanical properties on ordinary concrete, 2002.
[34] J.C. Committee, Recommendations for design and construction of high performance fiber reinforced cement composites with multiple fine cracks, Japan Soc. Civil Eng. (2008).
[35] B.P. Federation, Textile glass-woven fabric-determination of tensile breaking force and elongation at break by the strip method, London, 1995.
[36] J. Wang, Y. Wang, Y. Li, Research on fatigue performance of PVA-ECC under reciprocating action of the wheel pressure, Int. Conf. Intell. Syst. Res. Mechatron. Eng. (2015) 2075–2078.
[37] J. Wu, Development of Advanced Pavement Materials System for Blast Load, National University of Singapore, 2012.
[38] X.Z. Wang, Design of Airport Pavement, China Communications Press, Beijing, 2017.
[39] L. Liang, Q. Gu, G. Liu, R. Zhang, L. Jiang, Using ADAMS to assess dynamic load of pavement during aircraft landing, J. Southwest Jiaotong Univ. 47 (3) (2012) 502–508.
[40] AC 150/5320-6F. Airport pavement design and evaluation, 2016.
[41] R. Cojocaru, A. Radu, M. Budescu, Modelling of airport rigid pavement for complex configuration of landing gears and for a large spectrum of cement concrete, Interdisciplinary Res. Eng. 9 (2013) 235–242.
[42] Civil Aviation Administration of China. Statistical bulletin for the production of civil aviation airport in 2016. http://www.caac.gov.cn/XXGK/XXGK/TJSJ/201702/t20170224_42760.html.
[43] ASTM C597-09. Standard Test method for pulse velocity through concrete, 2009.
[44] S.A. Abo-Qudais, Effect of concrete mixing parameters on propagation of ultrasonic waves, Constr. Build. Mater. 19 (4) (2005) 257–263.
[45] A.M.T. Hassan, S.W. Jones, Non-destructive testing of ultra high performance fibre reinforced concrete (UHPFRC): a feasibility study for using ultrasonic and resonant frequency testing techniques, Constr. Build. Mater. 35 (2012) 361–367.
[46] R. Solis-Carcaño, E.I. Moreno, Evaluation of concrete made with crushed limestone aggregate based on ultrasonic pulse velocity, Constr. Build. Mater. 22 (6) (2008) 1225–1231.
[47] M. Sargolzahi, S.A. Kodjo, P. Rivard, J. Rhazi, Effectiveness of nondestructive testing for the evaluation of alkali–silica reaction in concrete, Constr. Build. Mater. 24 (8) (2010) 1398–1403.
[48] G. Singh, R. Siddique, Effect of waste foundry sand (WFS) as partial replacement of sand on the strength, ultrasonic pulse velocity and permeability of concrete, Constr. Build. Mater. 26 (1) (2012) 416–422.
[49] T. Planès, E. Larose, A review of ultrasonic Coda Wave Interferometry in concrete, Cem. Concr. Res. 53 (2013) 248–255.